International Journal of Science, Environment
and Technology, Vol. 1, No 2, 63 - 71, 2012

THREE-VALLEY MODEL OF ELECTRON TRANSPORT PROPERTIES IN BULK GASB AND $GA_{0.5}SB_{0.5}AS$ AT HIGH ELECTRIC FIELD

H. Arabshahi and Z. Moodi

Department of Physics, Payame Noor University, P. O. Box 19395-3697, Tehran, Iran
Email: hadi_arabshahi@yahoo.com

Abstract: Electron mobility simulation results are presented for bulk GaSb and $Ga_{0.5}Sb_{0.5}As$ based on a three-valley Monte Carlo model. Our velocity-field results at 300 K are in good agreement with available experimental data. It is found that GaSb exhibits an extremely low peak drift velocity at room temperature 0.27×10^5 ms^{-1}, at a doping concentration of 10^{17} cm^{-3} in comparison to GaAs. All dominant scattering mechanisms in the structure considered have been taken into account. For all materials, it is found that electron velocity overshoot only occurs when the electric field is increased to a value above a certain critical filed, unique to each material. This critical field is strongly dependent on the material parameters.
Keywords: Velocity overshoot; critical field; doping concentration; drift velocity.

1. Introduction

GaSb and related compounds have begun to generate a great deal of interest for a range of electronic and optical applications in recent years [1-3]. The growth of GaSb by metal organic chemical vapor deposition [4], and molecular beam epitaxy [5] has led to the development of resonant tunneling devices, infrared lasers, photo diodes [7], long wavelength infrared detectors, electro optic modulators and second-harmonic generators [8]. A rather unique feature of GaSb is that the L valley lies only about 85 meV above the Γ valley. Hence, it barely qualifies as a direct-gap semiconductor. It, therefore, becomes possible to easily convert the material into an indirect band structure either by applying suitably large magnetic fields, static pressure or through novel quantization effects. For instance, quantum confinement or the growth of a few mono layers of AlSb within a GaSb quantum well has been shown to push the Γ valley above the L valley energy minima. This

is useful, since the selection rule forbids inter subband absorption of normally incident light for a spherical constant-energy surface. However, with an ellipsoidal constant-energy surface, such as the L band of GaSb, inter subband transitions become allowed. This feature opens up possibilities for long-wavelength optical direction. Another advantage of GaSb is that it provides for type II band alignment in super lattices and quantum wells when used in conjunction with the InAs system. Such structures are being recognized as promising candidates for mid-infrared lasers due to the inherent suppression of internal electron-hole recombination. The Auger rates have also been shown to be greatly reduced in the GaSb based super lattices. Furthermore, as the GaSb/InAs share no common cation or anion, one can fabricate either an InSb-like or a GaAs-like interface simply by changing the growth sequence. Different vibrational properties are expected to result and the electronic properties of the confined carrier gas are correspondingly affected. In GaAs, the electron cloud tends to shift towards the arsenide atoms, which creates a dipole moment along the [111] axis. This causes the eight [111] surfaces to have differing concentrations of Ga and As atoms. As a result, the [111] planes are much tougher than expected. This toughening causes the [110] planes to be the primary fracture points. GaAs and GaSb also have a thermal conductivity that is less than one-third that of silicon and one-tenth that of copper, which makes it a poor conductor. The consequence of this poor conductivity is that the packing density of GaAs devices is limited by the thermal resistance of the substrate. Another thermal concern is the fact that brittle materials becomes ductile at around %35 of the melting point. Corresponding to 250 °C in GaAs, this marked drop in hardness and increase in fatigue could present serious problems for high temperature device operation. As the start of a program of work modeling high field transport and breakdown in GaSb and related materials, this paper presents the results of Monte Carlo simulations of electron transport in bulk GaSb and $Ga_{0.5}Sb_{0.5}As$. Most of the simulations have been carried out using a non-parabolic ellipsoidal valley model to describe transport in the conduction band. However, the simpler and less computationally intensive spherical parabolic band scheme has also been applied, to test the validity of this approximation. This article is organized as follows. Details of the conduction band parameters and the Monte Carlo simulation are presented in section 2, and results of steady-state simulations are interpreted in section 3.

2. Model Details

In this work, a three valley model of the first energy conduction bands of the empirical pseudopotential band structure for zincblende phase of $Ga_{0.5}Sb_{0.5}As$ and GaSb are chosen. The pseudopotential band structure shows the conduction band minimum to be located at the Γ point and lowest energy conduction band satellite valleys to occur at the L point and X symmetry points. In our Monte Carlo simulation, the four equivalent L valleys, the three equivalent X valleys, are represented by ellipsoidal, non-parabolic dispersion relationships of the following form,

$$E(k)[1+\alpha_i E(k)] = \frac{\hbar^2}{2}\left[\frac{k_x^2 + k_y^2}{m_\perp^*} + \frac{k_z^2}{m_\parallel^*}\right] \tag{1}$$

where $m^*_\perp$ and $m^*_\parallel$ are the transverse and longitudinal effective masses at the band edge and α_i is the non-parabolicity coefficient of the *i*-th valley. The band structure and material parameters necessary for calculating the scattering probabilities used in the present Monte Carlo simulation are given in table 1. Scattering mechanisms included in the simulation are acoustic deformation potential, pizoelectric and ionized impurity scattering. Elastic ionized impurity scattering is described using the screened Coulomb potential of the Brooks-Herring model. Furthermore, longitudinal optical phonon scattering, nonequivalent and, where applicable, equivalent inter-valley scattering events are taken into account among all valley types with the transfers assumed to be governed by the same deformation potential fields and the same phonon frequencies. Degeneracy effects are expected to be negligible over almost all of the temperature and electron concentration ranges of interest here and, hence, are not considered in the calculation.

In the case of $Ga_{0.5}Sb_{0.5}As$ the alloy scattering has also been included. Alloy scattering refers to the scattering due to the random distribution of the component atoms of the alloy among the available lattice sites. Harrison *et al.* [9] assumed that the alloy crystal potential can be described as a perfectly periodic potential which is then perturbed by the local deviations from this potential, due to the disordering effects in the alloy. Using the Harison model [9], the scattering rate due to the chemical disorder in a ternary alloy of electrons in a non-parabolic band is given by [9]

$$R_{alloy}(k) = \frac{4\sqrt{2\pi}m^{*3/2}r_0^6}{9\hbar^4}.\frac{x(1-x)(\Delta U)^2}{\Omega^2}\gamma^{1/2}(E)(1+2\alpha E) \quad (2)$$

where x denotes the molar fraction of one of the binary components of the alloy, Ω is the volume of the primitive cell and ΔU is the spherical scattering potential.

Electron particles in the ensemble Monte Carlo simulation occupy non-parabolic ellipsoidal valleys in reciprocal space, and obey Boltzmann statistics. Herring-Vogt transformations are used to map carrier momenta into spherical valleys when particles are drifted or scattered. The electric field equations are solved self-consistently with the electron transport using a finite difference method, and the device grid potentials are updated at each ensemble drift time step (1 femtosecond).

	GaSb	$Ga_{0.5}Sb_{0.5}As$
Density ρ (kgm^{-3})	5613	5200
Longitudinal sound velocity v_s (ms^{-1})	5630	5130
Low-frequency dielectric constant ε_s	15.69	11.4
High-frequency dielectric constant ε_∞	14.44	10.5
Acoustic deformation potential D(eV)	9.3	8.3
Polar optical phonon energy (eV)	0.029	0.09
Intervalley phonon energies (meV)	23.76	26

Table 1: Material parameter selections for GaSb and $Ga_{0.5}Sb_{0.5}As$ [3-5].

3. Results

The velocity-field characteristics, predicted by our model are shown in figure 1. For all cases, the temperature is 300 K and the donor concentration is $10^{17}cm^{-3}$. We see that each compound exhibits a peak in its velocity-field characteristic. The peak drift velocity for GaSb is around 0.2×10^5 ms^{-1}, while that for $Ga_{0.5}Sb_{0.5}As$ is about 1.4×10^5 ms^{-1}. At higher electric fields the drift velocity decreases, eventually saturating at around $0.1\times10^5 ms^{-1}$ for GaSb and at 0.6×10^5 ms^{-1} for $Ga_{0.5}Sb_{0.5}As$. The threshold fields are 1.5 kVm^{-1} and 2.5 kVm^{-1} for GaSb and $Ga_{0.5}Sb_{0.5}As$, respectively.

For GaSb the peak drift velocity occurs at a significantly lower electric field comparison

with other materials. The behaviour of GaSb can be explained in terms of the energy band structure. In particular, the different electron effective mass within the central valley (0.042 m_0 in GaSb versus 0.05 m_0 and 0.064 m_0 in $Ga_{0.5}Sb_{0.5}As$ and GaAs, respectively). Our results for $Ga_{0.5}Sb_{0.5}As$ are in fair agreement with Adashi's [28] report as it can be seen from figure 1.

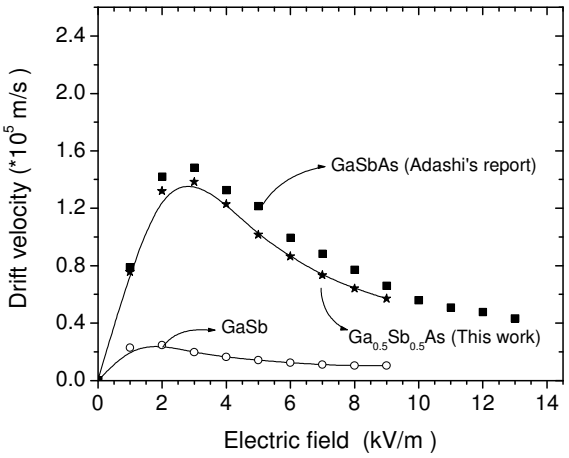

Figure 1: Calculated electron steady-state electron drift velocity in bulk GaSb and $Ga_{0.5}Sb_{0.5}As$ and as a function of applied electric field. The donor concentration is set to $10^{17}cm^{-3}$ and at temperature to 300 K.

The valley occupancies for the Γ, X and L valleys are illustrated in figure 2 and show that the inclusion of the satellite valleys in the simulation is important. Significant intervalley scattering into the satellite valleys occurs for fields above the threshold field for each material. This is important because electrons which are near a valley minimum have small kinetic energies and are therefore strongly scattered. It is apparent that intervalley transfer is substantially larger in GaSb over the range of applied electric fields shown, due to the combined effect of a lower Γ effective mass, lower satellite valley separation energy, and slightly lower phonon scattering rate within the Γ valley.

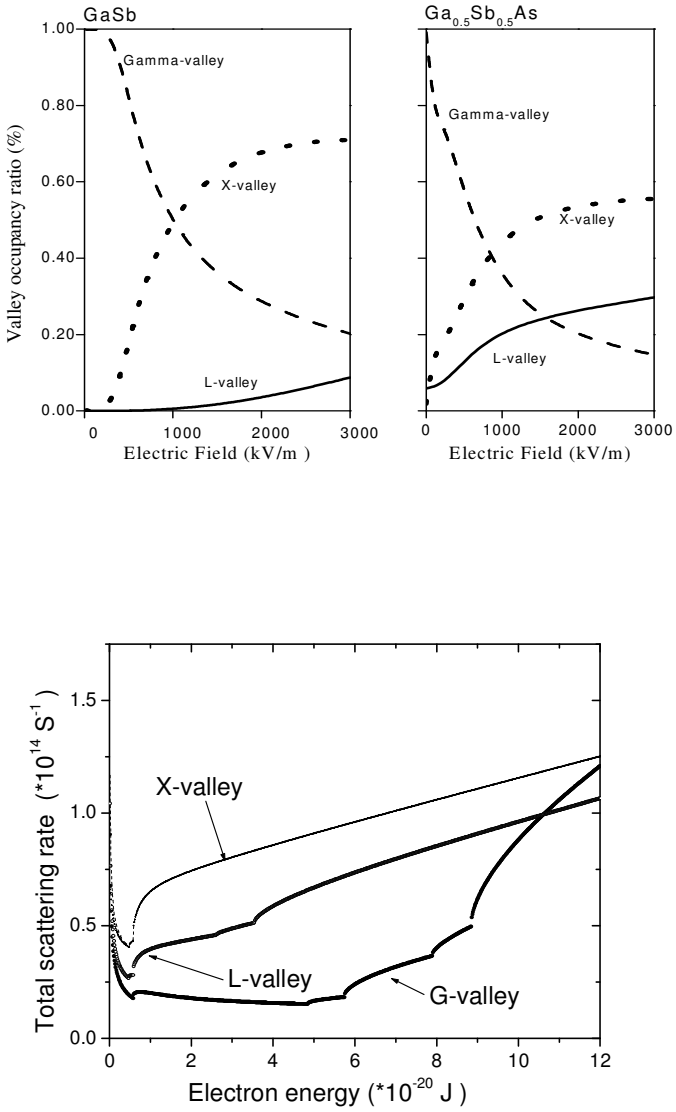

Figure 2: Comparison of the valley occupancies and their electron energies in GaSb and $Ga_{0.5}Sb_{0.5}As$ at room temperature. Total scattering rate in Γ, X and L valleys have also shown.

Figure 2 also shows, the electron energy functions and total scattering rate in Γ, X and L valleys for various materials in terms of electric field. These energy functions show similar features to those described previously and can be interpreted in terms of each material's band structure. We notice that the electron energy in the Γ valley increase until an energy unique to each material and after that decrease due to scattering to the satellite valleys.

Figure 3 shows the calculated electron drift velocity as a function of electric field strength for temperatures of 300, 400 and 500 K. The decrease in drift mobility with temperature at

low fields is due to increased intravalley polar optical phonon scattering whereas the decrease in velocity at higher fields is due to increased intra and intervalley scattering. It can be seen from the figure that the peak velocity also decreases and moves to higher electric field as the temperature is increased. This is due to the general increase of total scattering rate with temperature, which suppresses the electron energy and reduces the population of the satellite valleys. This latter effect is apparent from the fact that the electron population in the Γ-valley increases with temperature.

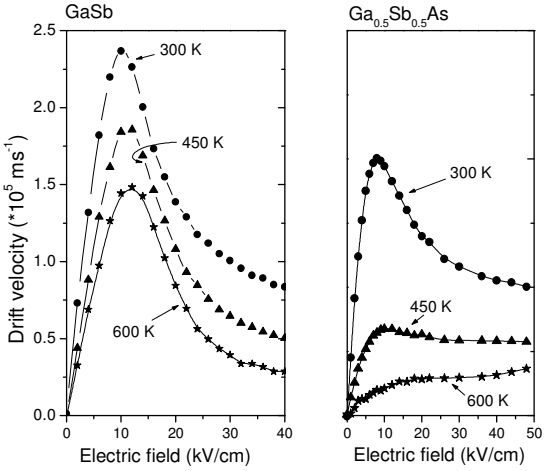

Figure 3: Calculated electron steady-state drift velocity in bulk GaSb and $Ga_{0.5}Sb_{0.5}As$ as a function of applied electric field at various lattice temperatures and assuming a donor concentration of 10^{17} cm^{-3}. The peak drift velocity decreases with increasing lattice temperature from 300 to 500 K in all structures.

Figure 4 shows how the velocity-field characteristic of $Ga_{0.5}Sb_{0.5}As$ and GaSb changes with impurity concentration at 300 K. It is clear that with increasing donor concentration, there are small changes in the average peak drift velocity and the threshold field. The results show the trend expected from increased ionized impurity scattering is in good general agreement with recent calculations by other workers.

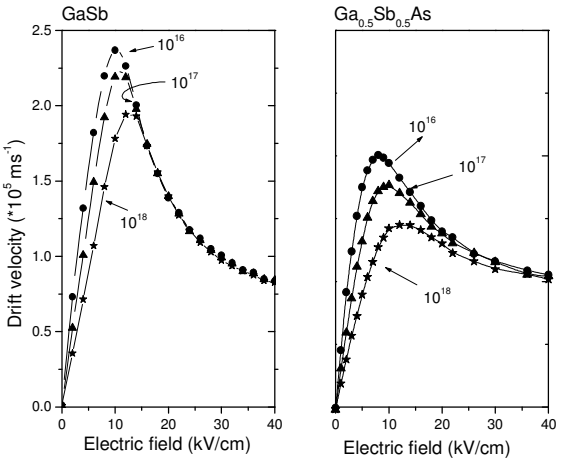

Figure 4: Electric field dependence of the drift velocity in GaSb and $Ga_{0.5}Sb_{0.5}As$ at 300 K for various donor concentration.

4. Conclusion

Electron transport at 300 K in bulk $Ga_{0.5}Sb_{0.5}As$ and GaSb have been simulated using an ensemble Monte Carlo simulation. Using valley models to describe the electronic band structure, calculated velocity-field characteristics are in fair agreement with other calculations. However, the peak electron drift velocity in GaSb occurs at a field of ~1 kVm^{-1}, 10 times lower than for $Ga_{0.5}Sb_{0.5}As$. This is a consequence of the smaller Γ-valley effective mass in the GaSb structure. This reduced valley effective mass permits substantial population of the upper valleys and velocity saturation at far lower electron temperatures than in $Ga_{0.5}Sb_{0.5}As$.

References

[1] R. M. Biefeld, "Monte Carlo Simulations of Staedy-State Transport in Wurtzite Phase GaN Submicrometer n^+nn^+ Diode", *Mater. Sci. Eng. R.*, 36, (2002), 105-111.

[2] R. Cusco, L. Artus, S. Henandez, J. Ibanez and G. Gonzalez-Diaz, "Comparison of High Field Electron Transport Properties in Wurtzite and Zincblende Phase GaN at Room Temperature", *Phys. Rev. B*, 65, (2001), 35210-35216.

[3] J. E. Maslar, W. S. Hurst and C. A. Wang, "The Effect of Strain Rate Variations on the Microstructure and Hot Deformation Behaviour of AA2024 Aluminium Alloy", *Appl. Spectrosc*., 61, (2007), 1093-1098.

[4] H. S. Bennett, H. Hung and A. Heckert, "Calculation of Electron Hall Mobility in GaSb, GaAs and GaN Using an Iterative Method", *J. Appl. Phys.,* 98, (2005), 103705-103709.

[5] F. Pascal, F. Delannoy, J. Bougnot, L. Gouskov and J. Kaoukab, "The Effect of Heat Treatment on Hot Deformation Behaviour of Al 2024", *J. Electron Matter*., 19, (1990), 187-192.

[6] K. F. Logenbach and W. I. Wang, "Comparison of Transport Ballistic Electron Transport in Bulk Wurtzite Phase 6H-SiC and GaN"*, Appl. Phys. Lett*., 59, (1991), 2427-2431.

[7] H. Kitabayashi, T. Waho and M. Yamamoto, "A Shock-Capturing Upwind Disceritization Method For Characterization of SiC MESFETs", *Appl. Phys. Lett*., 71, (1997), 512-517.

[8] D. H. Chow, R. H. Milnes, T. C. Hasebberg, A. R. Kost, Y. H. Zhang and L. West, "Temperature and Doping Dependencies of Electron Mobility in InAs, AlAs and AlGaAs under High Electric Fields", Appl. *Phys. Lett.*, 67, (1995), 3700-3707.

[9] J. Johnson, L. A. Samoska, A. C. Gossard and S. M. Johnson, "Monte Carlo Modeling of Hot Electron Transport in Bulk AlAs, AlGaAs and GaAs at Room Temperature", *J. Appl. Physics.,* 80, (1996), 1116-1120.

Received 28 April, 2012